Molecular Dynamics Simulation Studies of the Effect of Phosphocitrate on Crystal-Induced Membranolysis

Pranav Dalal,* Kimberly Zanotti,* Andrzej Wierzbicki,† Jeffry D. Madura,* and Herman S. Cheung‡
*Department of Chemistry and Biochemistry Center for Computational Sciences, Duquesne University, Pittsburgh, Pennsylvania 15282; †Department of Chemistry, University of South Alabama, Mobile, Alabama 36688; and ‡Department of Biomedical Engineering, University of Miami, and Geriatric Research, Education, and Clinical Center, Veterans Administration Medical Center, Miami, Florida 33135

ABSTRACT In this study, following our earlier work on calcium pyrophosphate dihydrate (CPPD) crystal-induced membranolysis, we demonstrate, using the CHARMM method of molecular dynamics simulation, the protective role of phosphocitrate (PC) against solvated dimyristoyl phosphatidylcholine phospholipid bilayer disintegration on contact with the CPPD crystal. Our molecular dynamics simulations studies show that coverage of the CPPD crystal with a layer of phosphocitrate molecules results in the conservation of phospholipid bilayer integrity. We show that the rupture of the lipid bilayer in presence of CPPD and the protective effect of PC are primarily due to electrostatic interactions. The protective role of PC, which may also play an important and potentially therapeutic function against crystal-induced membranolysis is also discussed.

INTRODUCTION

Inflammation in the inflammatory diseases such as arthritis is proposed to be due to the rupture of the lysosome phospholipid membrane and the release of lysosomal enzymes into the cytoplasm. The rupture of the membrane or membranolysis is usually accompanied by the crystal deposition near the membrane (1–4). Calcium pyrophosphate dihydrate (CPPD) crystal is one of the most common forms of pathologic articular mineral, and its deposition leads to pseudogout, an inflammatory disease. The crystal deposition increases in prevalence with aging (50% at the age of 90 years) and occurs frequently in degenerative joints. Although deposition occurs frequently in noninflammatory osteoarthritic (OA) joints, it can be phlogistic, causing acute attacks of pseudogout.

Pathologic crystals (e.g., CPPD) that induce membranolysis can be differentiated from nonpathologic crystals by their surface charge and topography. Pathologic crystals, also known as membranolytic crystals such as monosodium urate, CPPD, and the α-quartz form of silicon dioxide, are irregular and possess a high density of negatively charged groups as compared to nonmembranolytic smooth surface crystals, e.g., diamond dust and the anatase form of silicon dioxide. The less negatively surface-charged brushite and hydroxyapatite crystals are not often associated with acute inflammation (5).

Until recently, only indirect evidence of the crystal-membrane interactions have been presented. For example, it has been demonstrated that the adhesion of calcium oxalate monohydrate crystals involves anionic sites on the surface of renal epithelial cells (6,7). In another related study (8) involving different classes of anionic crystals, namely hydroxyapatite, it has been also speculated that the interaction between renal epithelial cells and hydroxyapatite crystal surfaces involves negatively charged molecules protruding from the apical surface of the plasma membrane. However, very recently, employing computational techniques, we have presented direct evidence that the crystal-membrane interaction leads to a rupture of the lipid bilayer (1). We have proposed that the interactions between the surface of the CPPD crystal and the extracellular layer of the hydrated dimyristoyl phosphatidylcholine (DMPC) phospholipid bilayer may lead to decoupling of the external layer from the intracellular side of the membrane. In turn, a local thinning of the layer on the intracellular side of the membrane occurs, which favors water penetration, leading to membranolysis.

Understanding these interactions at the molecular level is extremely helpful, not only to elucidate the molecular nature of cell-crystal interaction, but also to aid in design of therapeutic agents that could diminish such an interaction. There is already some experimental evidence that phosphocitrate, a polyanion, protects from crystal-induced polymorphonuclear leukocyte membranolysis (9). The CPPD crystal surface, although neutral, contains loci of both positive and negative charges, and is able to attract complementarily charged molecular species, like the highly negatively charged (-4) phosphocitrate anion. Studies of interactions between ionic crystals and phospholipid bilayers show that these interactions can be modified by polyanions like phosphocitrate, citrate, polyasparate, and polyglutamate. Our earlier molecular modeling studies show that phosphocitrate could be used as a powerful inhibitor of the (010) crystal surfaces of CPPD crystal (10).

In this work we have undertaken computational modeling studies to determine the effect of phosphocitrate on the CPPD-induced membranolysis of the DMPC phospholipid bilayers. We show that phosphocitrate greatly inhibits the CPPD-induced membranolysis.

Submitted December 21, 2004, and accepted for publication July 1, 2005.

Address reprint requests to Andrzej Wierzbicki, E-mail: awierzbi@jaguar1.usouthal.edu.

0006-3495/05/10/2251/07 $2.00

doi: 10.1529/biophysj.104.058503

METHODS

The generation of the solvated DMPC lipid bilayer with a CPPD crystal and the lipid/water interface is described in detail in our earlier study (1). The same lipid bilayer system was employed in these simulations. The solvated lipid bilayer system used in the simulations was 48 × 32 × 88 Å. In this study we employed a slightly different slab of the CPPD crystal. To maintain the neutrality of the CPPD-PC system, we prepared the CPPD crystal slab, which had a total charge of +32. Subsequently, using Monte Carlo docking, eight phosphocitrate ions (−4 charge each) were docked on the crystal in a sequential fashion. Initially, a phosphocitrate ion was placed >10 Å away from the CPPD crystal. A Monte Carlo simulation was performed at this point (5000 steps) to identify the most favorable position and orientation of the phosphocitrate ion by determining the most favorable interaction energy of the phosphocitrate ion on the CPPD crystal. After the docking of the first phosphocitrate ion, a second phosphocitrate ion was placed on the resulting system in a similar fashion. We found that both the phosphocitrate ions were the same distance from the crystal and oriented identically in space. Hence, for docking of subsequent phosphocitrate ions, the distance of the ion and its orientation were held fixed. With the aid of such Monte Carlo docking simulations, we covered the CPPD surface with eight phosphocitrate ions (total charge = −32). The resulting system was neutral (CPPD crystal = +32 and phosphocitrate ions = −32).

The complex of CPPD crystal and eight phosphocitrate ions was placed at the lipid bilayer/water interface. The initial position of the crystal was determined from our previous study. However, because the height of phosphocitrate ion is 5 Å, we moved the CPPD-phosphocitrate ion complex 5 Å away from the lipid bilayer from the initial position. During the simulation, the position of CPPD-PC complex was held fixed. In this study the simulation time for the bilayer and the bilayer-CPPD-PC was 1.2 ns. Other simulation details are described in detail in our previous study (1).

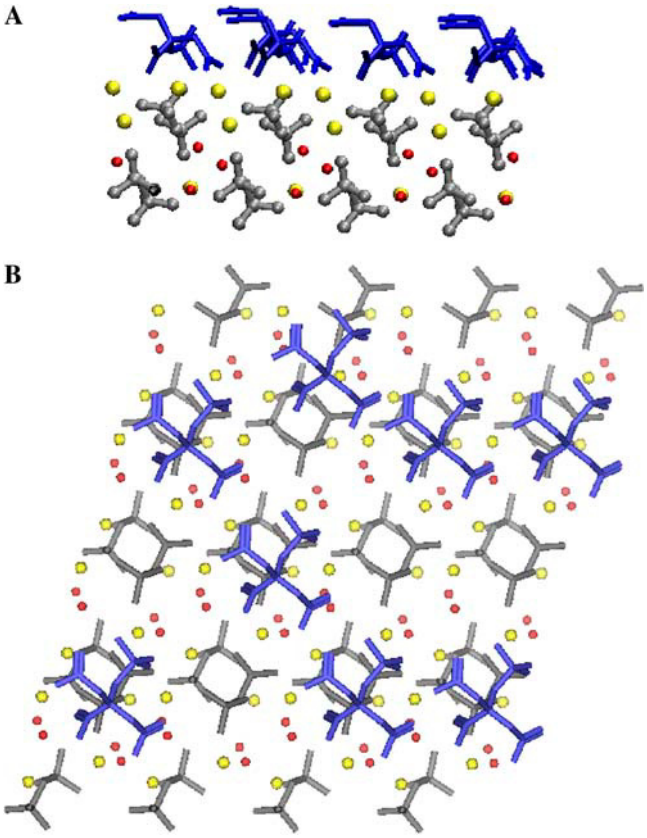

FIGURE 1 (*A*) Side view of the CPPD-PC complex. The CPPD crystal (*bottom*) complexed with eight phosphocitrate ions (*top*) is shown. The crystal is shown in ball-and-stick configuration, whereas the PC is shown in stick configuration. The hydrogens are not shown for clarity. The color coding is as follows: pyrophosphate, gray; water, red; calcium, yellow; and phosphocitrate, blue. (*B*) Top view of the CPPD-PC complex. The top view of the CPPD crystal complexed with eight phosphocitrate ions is shown. The oxygen atoms of the water molecules in the crystal and the calcium ions in the crystal are shown in ball configuration. The pyrophosphate part of the CPPD crystal and PC ions are shown in stick configuration. The hydrogens are not shown for clarity. The color coding is as follows: pyrophosphate, gray; water, red; calcium, yellow; and phosphocitrate, blue.

RESULTS

Shown in Fig. 1 are the side and top views of the complex of CPPD crystal and eight phosphocitrate ions. As is evident from the figure, the PC ions occupy similar lattice positions on the crystal. This particular orientation of PC ions on the CPPD crystal allows the maximum interaction between the electronegative oxygen atoms of the PC ions and the positive calcium ions of the CPPD crystal. This complex of CPPD-PC was employed in our simulations.

In our previous study (1), the molecular dynamics simulations of solvated lipid bilayer in the presence of the CPPD crystal have shown that the phospholipid bilayer disintegrates during the 600-ps simulation time (Fig. 6 in Wierzbicki et al. (1)). Furthermore, we observed that the crystal stabilizes the adjacent leaflet, while destabilizing the lipid leaflet on the opposite side. We also observed that the water penetrates the bilayer from the side, which is opposite to the crystal. In this study we placed CPPD at the same distance from the bilayer as observed in the CPPD-PC system. We observed similar leakage of the bilayer as the earlier simulations (1).

Fig. 2 shows the results from this study in which the CPPD-PC complex was placed at the lipid/water interface of the solvated lipid bilayer system. Shown in this figure are the snapshots (200 ps apart) from our molecular dynamics simulations. As observed from the figure, the lipid bilayer integrity is maintained. We observe that the waters do not penetrate the lipid bilayer. This clearly indicates that PC has a protective effect on the CPPD-induced lipid bilayer leakage.

Fig. 3 depicts number profile plots in which we have calculated the average number of the water oxygen and lipid nitrogen atoms in the solvated lipid bilayer-CPPD-PC over 0–200, 200–400, 400–600, and 1000–1200 ps. These plots show the number of water O atoms (Fig. 3 *A*) and the headgroup N atoms of the lipid bilayer (Fig. 3 *B*) across the water/lipid interface in the solvated lipid bilayer-CPPD-PC system. These figures clearly show that the water molecules are outside the bilayer and do not penetrate into the bilayer throughout the simulation. The headgroup N atoms are distributed evenly, and the majority of them lie in the same plane (Fig. 3 *B*). These properties are also clearly evident from Fig. 2. Fig. 3, *A* and *B*, show that in the presence of the

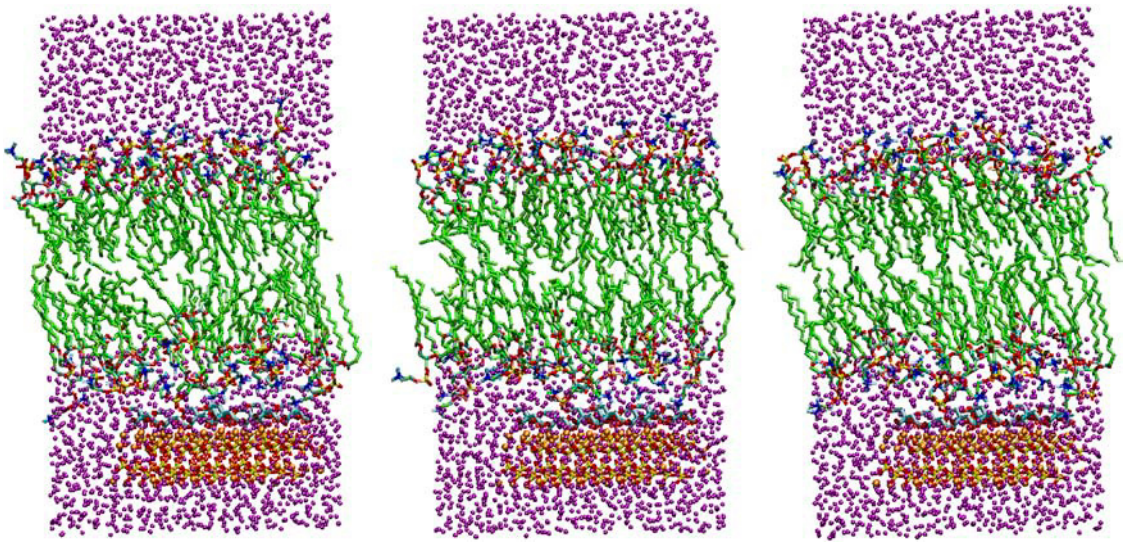

FIGURE 2 Snapshots from the simulation of a solvated lipid bilayer with a CPPD crystal at one of the lipid/water interfaces are shown. The magenta spheres indicate the oxygen atoms of the water molecules. The lipid molecules are shown as chains. The crystal is depicted at the lower lipid/water interface using ball-and-stick scheme, and the phosphocitrate is shown in stick configuration. The color scheme for the lipid headgroups, CPPD, and PC is: oxygen, red; phosphorus, yellow; carbon, cyan; nitrogen, blue; and calcium, gold. The snapshots shown here are 200 ps apart, time advancing from left to right.

CPPD crystal covered with a layer of PC, the phospholipid bilayer remains remarkably stable even when the simulation time is doubled from 600 to 1200 ps. Because doubling the simulation time does not produce any further changes in our solvated lipid bilayer-CPPD-PC system, we will use the data obtained for the first 600 ps of our simulation time to more directly compare the results of this study with our earlier 600-ps study of the solvated lipid bilayer-CPPD system without PC (1).

In our previous study, in the simulation involving only the lipid bilayer (without the CPPD crystal), the diffusion coefficient of the nitrogen atoms of the lipid headgroup was relatively similar. For the bottom layer, we calculated a value of $0.55 \times 10^{-2} \pm 0.9 \times 10^{-4}$ Å^2/ps and for the top layer, $0.69 \times 10^{-2} \pm 0.16 \times 10^{-3}$ Å^2/ps. However, the values were quite different for the simulations in which we placed the crystal at the bottom lipid leaflet. In those simulations, for the bottom layer (interacting with crystal) we obtained a value of $0.16 \times 10^{-2} \pm 0.1 \times 10^{-4}$ Å^2/ps, whereas for the top layer we obtained a value of $2.4 \times 10^{-2} \pm 0.21 \times 10^{-3}$ Å^2/ps. Thus, we observed that the lipid headgroups near the crystal had a reduced mobility, and the ones on the far end had an increased mobility compared to a solvated lipid bilayer in the absence of the crystal. Similarly, we measured the headgroup mobility in the current simulations. In this study, we determined that the diffusion coefficient of the nitrogen atoms of the lipid headgroups near the CPPD-PC complex was $0.42 \times 10^{-2} \pm 0.55 \times 10^{-4}$ Å^2/ps, whereas for those on the opposite side it was $0.31 \times 10^{-1} \pm 0.94 \times 10^{-3}$ Å^2/ps. Thus, we observe in this simulation that, in the presence of PC, the mobility of the lower (external) layer is almost the same as for the solvated bilayer. The upper (internal) layer on the opposite side has a higher mobility, similar to that observed in the simulation of lipid bilayer in the presence of the CPPD crystal (Table 1). However, it must be noted here that the ratio of mobilities between the upper and lower layers decreased from 15 to 7.4 for the bilayer-CPPD and bilayer-PC-CPPD, respectively. Despite the elevated mobility of the opposite leaflet, the bilayer-PC-CPPD system does not break, which indicates that the underlying mechanism is not mobility driven.

To verify that the lipid bilayer breakdown for bilayer-CPPD system is not caused by difference in the lipid mobility in the upper and lower layers, as we proposed earlier in Wierzbicki et al. (1), we did a simulation of solvated lipid bilayer in which we kept the headgroups of the bottom leaflet fixed (diffusion coefficient = 0 Å^2/ps). We observed that the headgroups on the opposite side showed no significant increase in the mobility and the lipid bilayer was intact during the simulation time. These results suggest that the breakdown of the integrity of the lipid bilayer in the bilayer-PC system is not due to change in mobility of the lipid headgroups.

In our simulations of the bilayer-CPPD system, we observed that the penetrating water molecules were all oriented in the same way, with oxygen atoms pointing at the crystal and hydrogen atoms pointing away from the crystal. This led us to propose an alternative mechanism of the breakdown of the lipid bilayer, which could be driven by the electrostatic interactions instead. Under this hypothesis, the electrostatic field induced by the crystal should alter the lipid headgroup dipole orientation and hence its orientation with respect to

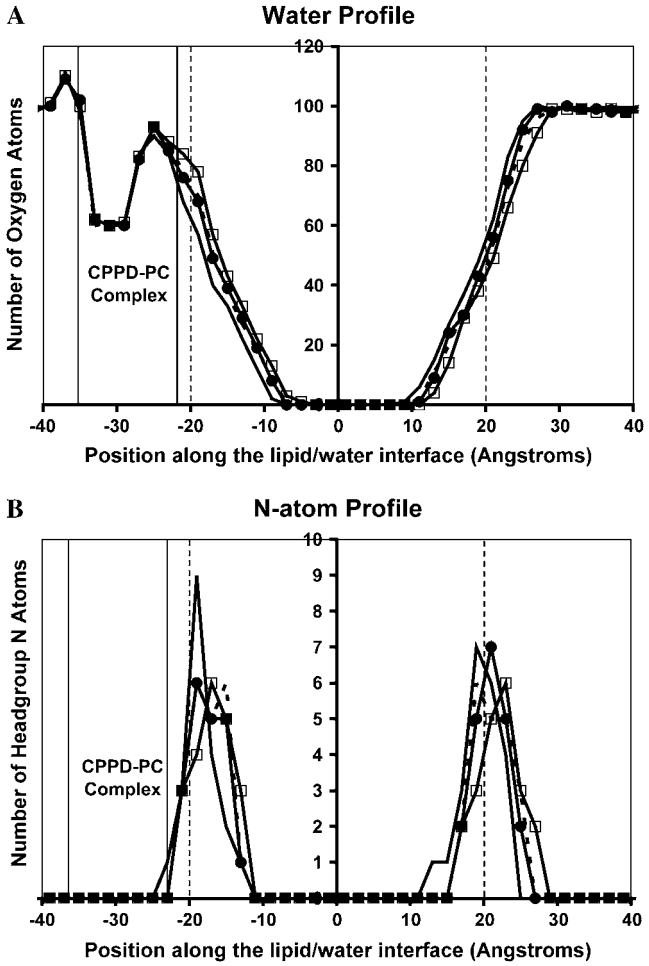

FIGURE 3 Density profiles of water and lipid molecules. Fig. 3, *A* and *B*, show the number of the oxygen atoms of the water molecules and the number of lipid headgroup nitrogen atoms, respectively, along the water/lipid interface when the CPPD/PC complex is present at the bottom lipid layer. The data are presented as time-averaged series. The averages from 0 to 200 ps (*solid line*), 200–400 ps (*solid line* with *circles*), 400–600 ps (*dashed line*), and 1000–1200 ps (*solid line* with *open squares*) are presented. The *x* axis depicts the position along the lipid/water interface, 0 being the center of the bilayer, whereas the number of atoms is plotted on the *y* axis. The negative coordinates are below the center of the bilayer, and the positive coordinates are above the center (see Fig. 2). The dashed lines within the graph indicate the position of the bilayer-water interface.

the bilayer normal. To test this hypothesis, we calculated the angle between the lipid bilayer normal and the vector defined by the P and N atoms of the lipid headgroup. This angle was calculated for individual lipid headgroups for bottom and top leaflets from coordinates saved every 1 ps. The data from the individual lipid molecules were combined together for the top and the bottom leaflet and subsequently histogrammed (Fig. 4). These results show that the distribution of the angles for the solvated bilayer and the bilayer-PC-CPPD system are symmetrically distributed and highly similar for both the leaflets. On the other hand, the distribution for the bilayer-CPPD system is different. The distribution of the angles for the top leaflet is shifted to the left, reflecting the electrostatic force on the headgroup due to the crystal. Interestingly, the angle distribution is affected to a much lesser extent for the bottom leaflet. These results and observations lead us to conclude that the waters and lipid headgroups are electrostatically affected by the crystal and that waters get pulled through the bilayer leading to breakdown of the integrity of the bilayer, which leads to the increased mobility of the lipid headgroups.

DISCUSSION

In the first study of its kind (1), we recently showed clearly that the CPPD crystal causes the loss of lipid bilayer integrity. This model now provides us with a great tool in elucidating the mechanism of the crystal-induced cell damage. This is a great step forward in understanding and treating inflammatory diseases such as arthritis.

We have previously shown (10) that phosphocitrate binds to the specific faces of CPPD and proposed that this induces morphological changes that may lead to diminished crystal growth or its total cessation. The orientation of PC binding to CPPD crystal obtained in our previous study is slightly different from the one obtained in the current study. However, the main features are identical: the phosphate group of PC places itself in the position at the surface that would be occupied by pyrophosphate ion, assuming crystal lattice would have continued upward. Furthermore, the electronegative carboxylate groups of PC are placed near the positive calcium ions of CPPD.

In vitro experiments have shown that PC inhibits CPPD crystal formation in isolated articular cartilage vesicles. Cheung et al. (11) showed that PC (10–100 μM) blocked both ATP-dependent and -independent mineralization in articular cartilage vesicles. PC has also been shown to be a potent in vitro inhibitor of basic calcium phosphate (BCP) (12) (another pathologic articular mineral) and calcium oxalate monohydrate (13,14) crystal formation.

TABLE 1 Mobility of lipid headgroups

	Phospholipid bilayer system (Å^2/ps)	Phospholipid bilayer-CPPD system (Å^2/ps)	Phospholipid bilayer-PC-CPPD system (Å^2/ps)	Phospholipid bilayer (bottom layer fixed) (Å^2/ps)
Top layer	$0.69 \times 10^{-2} \pm 0.16 \times 10^{-3}$	$2.4 \times 10^{-2} \pm 0.21 \times 10^{-3}$	$3.1 \times 10^{-2} \pm 0.94 \times 10^{-3}$	$0.98 \times 10^{-2} \pm 0.54 \times 10^{-3}$
Bottom layer	$0.55 \times 10^{-2} \pm 0.09 \times 10^{-3}$	$0.16 \times 10^{-2} \pm 0.01 \times 10^{-3}$	$0.42 \times 10^{-2} \pm 0.05 \times 10^{-3}$	0

The average diffusion coefficient values are provided for the N atoms of the lipid headgroups for each layer of the lipid bilayer. The CPPD and CPPD/PC complexes were placed adjacent to the bottom layer.

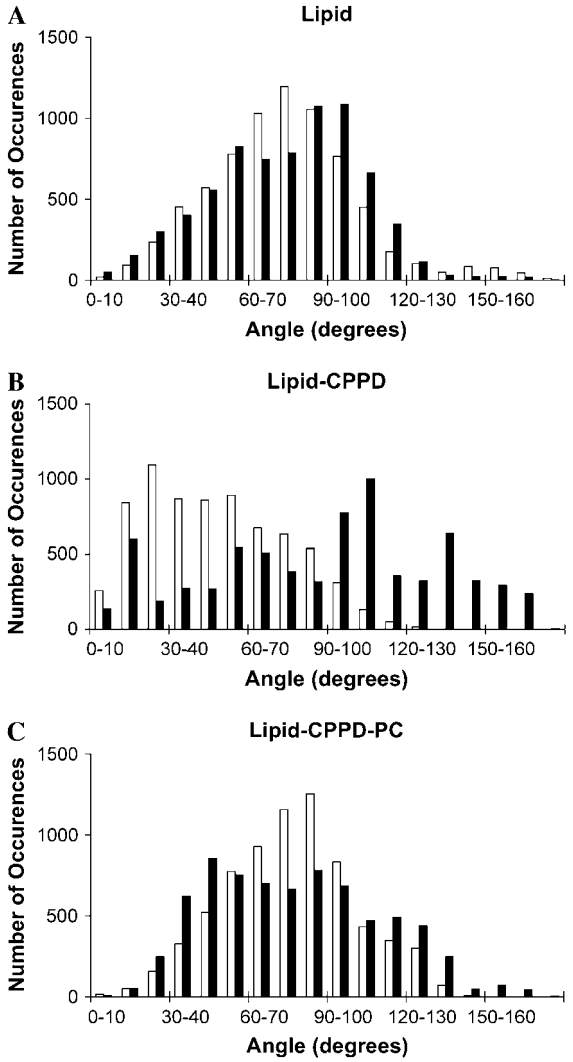

FIGURE 4 Distribution of the angle between the bilayer normal and lipid headgroup (vector defined by P and N atoms of the headgroup). The distribution of the angle between the bilayer normal and vector defined by P and N atoms of the headgroup is plotted. The number of occurrences is plotted on the *y* axis and histogram bins on the *x* axis. The solid bars represent the bottom leaflet (in contact with CPPD and CPPD-PC systems), and the open bars represent the top leaflet of the lipid bilayer. Plots for (*A*) lipid, (*B*) lipid-CPPD, and (*C*) lipid-CPPD-PC systems are shown.

It has been demonstrated that PC inhibits CPPD and BCP crystal-induced mitogenesis and metalloproteinase synthesis and secretion by fibroblasts and chondrocytes (15,16). There are other in vitro studies investigating the preventive effect of PC on CPPD- and BCP-induced biological damage. Moreover, as mentioned earlier, it has also been shown that PC binds these crystals. However, this is the first computational study that clearly shows the protective effect of PC on CPPD-induced lipid bilayer breakdown.

The results reported in this study suggest that the CPPD-induced lipid bilayer leakage is not due to changes in mobility as we thought previously (1). Instead, we propose that the CPPD induces an electrostatic field distribution across the lipid bilayer, which allows the water molecules to move across the bilayer toward the crystal. Hence, when PC is bound to the CPPD crystal, this electrostatic field is shielded and the waters are not pulled toward the crystal. To investigate the role that the electrostatic field plays in the CPPD-induced bilayer rupture, we have calculated the electrostatic potential maps for the system under the investigation. Fig. 5 displays the GRASP (17) electrostatic potential maps for the hydrated phospholipid bilayer alone (Fig. 5 *A*), the hydrated phospholipid bilayer-CPPD system (Fig. 5 *B*), and the hydrated phospholipid bilayer-CPPD-PC system (Fig. 5 *C*), taken after 200 ps of molecular dynamics simulation. For the hydrated bilayer (Fig. 5 *A*) the electrostatic field is essentially slightly positive (*light blue*) everywhere except within the layer of the phosphate headgroups of the DMPC assembly. Introduction of the CPPD crystal slab (Fig. 5 *B*) results in dramatic changes in the distribution of electrostatic potential within the bilayer. As one can see from this picture, the crystal slab generates an oriented, dipole-like electrostatic field distribution in the immediate vicinity of the crystal, with the positive and negative areas of electrostatic potential clearly separated by the crystal slab. We can see that this dipole-like field extends deeply into the bilayer with the electrostatic field distribution within the bilayer being positive (*blue*) on the CPPD crystal side of the bilayer and negative on the opposite side of the bilayer (*red*). Thus, this ''induced polarization'' of the bilayer seems to have an opposite direction to the dipole field of the slab, and clearly one can see evidence of a gradient of the electrostatic potential across the bilayer. The presence of this directional electrostatic field may explain why, as it was mentioned earlier in our simulations of the bilayer-CPPD system, we observed that the penetrating water molecules were all oriented in the same way, with oxygen atoms pointing at the crystal and hydrogen atoms pointing away from the crystal. When the CPPD crystal slab is covered with phosphocitrate, the electrostatic field of the crystal slab is dramatically altered (Fig. 5 *C*). The positive side of this field (*blue*) stays localized very close to the surface of the crystal, and the electrostatic potential inside the bilayer resembles very closely that of the free bilayer (Fig. 5 *A*), staying in general on the slightly positive side of the potential (*light blue*) as in Fig. 5 *A*. There is no evidence of the electrostatic potential gradient in the direction perpendicular to the crystal surface. The results discussed above clearly demonstrate that phosphocitrate molecules distributed at the CPPD crystal surface can protect the structural integrity of the phospholipid bilayer by not allowing the electrostatic field of the crystal to penetrate into the bilayer.

In conclusion, we propose that the CPPD-induced bilayer rupture is more of an electrostatic-induced and less of a mechanics-induced phenomenon. More importantly, we show that phosphocitrate can prevent CPPD-induced membranolysis of the phospholipid bilayers. Results of this study

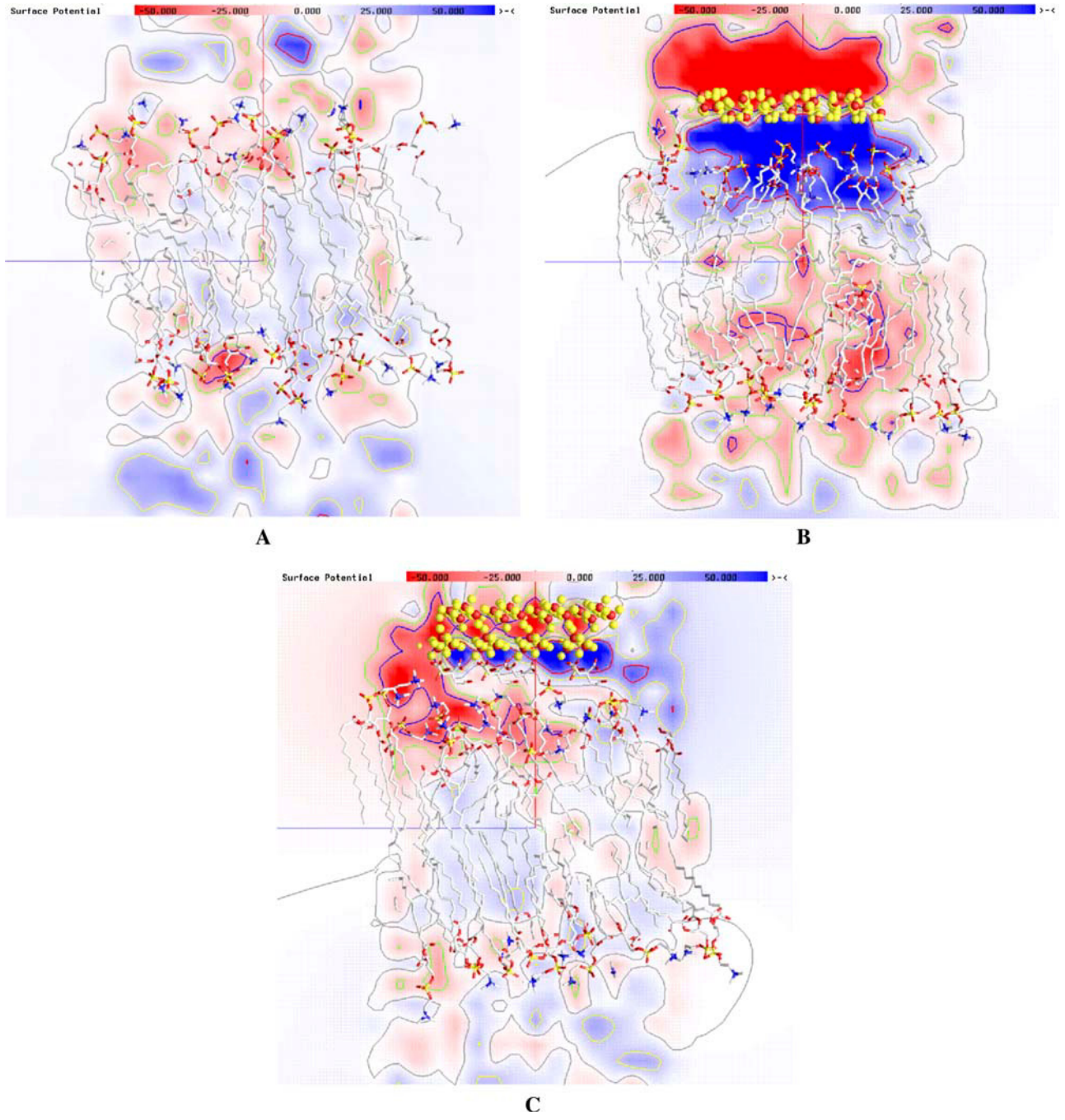

FIGURE 5 GRASP (17) electrostatic potential plots for (*A*) hydrated phospholipid bilayer, (*B*) hydrated phospholipid bilayer and the CPPD crystal, (*C*) hydrated phospholipid bilayer and PC-CPPD system. The plots show the electrostatic potential distribution after 200 ps of molecular dynamics simulation in a plane through the center of the collection of molecules. The in-plane line contours are at (−30, −15, 0, 15, 30), (*blue*, *green*, *gray*, *yellow*, and *red*), respectively, and the in-plane colors range is (−50,0,50) in units of kT/e (= 0.591 kcal/e).

provide a molecular model that explains why subjecting the CPPD crystals in vivo to phosphocitrate could significantly diminish the interactions between the CPPD crystals and phospholipid bilayers and thus phosphocitrate could serve as a potentially powerful therapeutic agent in crystal-induced arthritic diseases.

We thank Dr. Anthony Nicholls for his help in generating the GRASP (17) images shown in Fig. 5.

We acknowledge Pittsburgh Supercomputing Center (grants MCA02N008P and MCB020003P) for its generous allowance of the supercomputer time. We also acknowledge the National Institutes of Health grant (AR38421-14) and Veterans Administration Merit Review for supporting this research.

REFERENCES

1. Wierzbicki, A., P. Dalal, J. D. Madura, and H. S. Cheung. 2003. Molecular dynamics simulation of crystal-induced membranolysis. *J. Phys. Chem. B.* 107:12346–12351.
2. Ryan, L. M., and D. J. McCarty. 1997. Calcium pryophosphate dihydrate crystal deposition disease; pseudogout; articular chondrocalcinosis. *In* Arthritis and Allied Conditions, 13th Ed. W. J. Koopman, editor. Williams & Wilkins, Baltimore, MD. 2103–2125.
3. Ryan, L. M., and H. S. Cheung. 1999. The role of crystals in osteoarthritis. *Rheum. Dis. Clin. North Am.* 25:257–267.
4. Mandel, N. S. 1976. The structural basis of crystal induced membranolysis. *Arthritis Rheum.* 19:439–445.
5. Terkeltaub, R. A. 1997. Pathogenesis and treatment of crystal-induced inflammation. *In* Arthritis and Allied Conditions, 13th Ed. W. J. Koopman, editor. Williams & Wilkins, Baltimore, MD. 2085–2102.
6. Lieske, J. L., F. G. Toback, and S. Deganello. 1996. Face specific adhesion of calcium oxalate dihydrate crystals in renal epithelial cells. *Calcif. Tissue Int.* 58:195–200.
7. Lieske, J. C., R. Norris, and F. G. Toback. 1997. Adhesion of hydroxiapatite crystals to anionic sites on the surface of renal epithelial cells. *Am. J. Physiol.* 273:F224–F232.
8. Lieske, J. C., R. Leonard, H. Swift, and F. G. Toback. 1996. Adhesion of calcium oxalate monohydrate crystals to anionic sites on the surface of renal epithelial cells. *Am. J. Physiol.* 270:F192–F199.
9. Sallis, J. D., R. Shankar, B. Rees, and R. Thomson. 1989. Protection of crystal-induced polymorphonuclear leukocyte membranolysis by phosphocitrate. *Biochem. Med. Metab. Biol.* 41:56–63.
10. Wierzbicki, A., and H. S. Cheung. 1998. Molecular modeling of inhibition of crystals of calcium pyrophosphate dihydrate by phosphocitrate. *J. Mol. Struct.* (*THEOCHEM*). 454:287–297.
11. Cheung, H. S., I. V. Kurup, J. D. Sallis, and L. M. Ryan. 1996. Inhibition of calcium pyrophosphate dihydrate crystal formation in articular cartilage vesicles and cartilage by phosphocitrate. *J. Biol. Chem.* 271:28082–28085.
12. Shankar, R., S. Crowden, and J. D. Sallis. 1984. Phosphocitrate and its analogue N-sulpho-2-amino tricarballylate inhibit aortic calcification. *Atherosclerosis.* 52:191–198.
13. Wierzbicki, A., C. S. Sikes, J. D. Sallis, J. D. Madura, E. D. Stevens, and K. L. Martin. 1995. Scanning electron microscopy and molecular modeling of inhibition of calcium oxalate monohydrate crystal growth by citrate and phosphocitrate. *Calcif. Tissue Int.* 56:297–304.
14. Sallis, J. D., N. F. G. Parry, J. D. Meehan, H. Kamperman, and M. E. Anderson. 1995. Controlling influence of phosphocitrate in vitro and in vivo on calcium oxalate crystal formation and growth. *Scanning Microsc.* 9:127–136.
15. Cheung, H. S., J. D. Sallis, P. G. Mitchell, and J. A. Struve. 1990. Inhibition of basic calcium phosphate crystal-induced mitogenesis by phosphocitrate. *Biochem. Biophys. Res. Commun.* 171:20–25.
16. Cheung, H. S., J. D. Sallis, and J. A. Struve. 1996. Specific inhibition of basic calcium phosphate and calcium pyrophosphate crystal-induction of metalloproteinase synthesis by phosphocitrate. *Biochim. Biophys. Acta.* 1315:105–111.
17. Nicholls, A., K. A. Sharp, and B. Honig. 1991. Protein folding and association: insights from the interfacial and thermodynamic properties of hydrocarbons. *Proteins.* 11:281–296.